

First observations of CN(2-1), HCO⁺(3-2) and C₂H(3-2) emission lines in the Perseus cluster: constraints on heating mechanisms in the cluster gas.

E. Bayet^{1*}, S. Viti², T. W. Hartquist³ and D.A. Williams²

¹*Sub-Department of Astrophysics, University of Oxford, Denys Wilkinson Building, Keble Road, Oxford OX1 3RH*

²*Department of Physics and Astronomy, University College London, Gower Street, London WC1E 6BT, UK*

³*School of Physics and Astronomy, University of Leeds, Leeds LS2 9JT, UK*

Accepted ; Received ; in original form

ABSTRACT

We present the first observations of emission lines of CN(2-1), HCO⁺(3-2) and C₂H(3-2) in the Perseus cluster. We observed at two positions: directly at the central galaxy, NGC 1275 and also at a position about 20'' to the east where associated filamentary structure has been shown to have strong CO emission. Clear detections in CN and HCO⁺ transitions and a weak detection of the C₂H transition were made towards NGC 1275, while weak detections of CN and HCO⁺ were made towards the eastern filamentary structure. Crude estimates of the column densities and fractional abundances (mostly upper limits) as functions of an unknown rotational temperature were made to both sources. These observational data were compared with the outputs of thermal/chemical models previously published by Bayet et al. (2011) in an attempt to constrain the heating mechanisms in cluster gas. We find that models in which heating is dominated by cosmic rays can account for the molecular observations. This conclusion is consistent with that of Ferland et al. (2009) in their study of gas traced by optical and infrared radiation. The cosmic ray heating rate in the regions probed by molecular emissions is required to be at least two orders of magnitude larger than that in the Milky Way.

Key words: Astrochemistry - ISM:abundances - galaxies: intergalactic medium - Galaxies: clusters: individual:Perseus - galaxies: individual: NGC 1275 - Galaxies: cooling flows

1 INTRODUCTION

The Perseus Cluster is one of the nearest galaxy clusters and is the brightest X-ray cluster in the sky. The cluster and its central galaxy NGC 1275 have been the focus of intense study for many years, at X-ray, optical, IR and millimetre wavelengths. The first molecular detections were of CO rotational emission towards the centre of NGC 1275 (Lazareff et al. 1989; Mirabel, Sanders & Kazes 1989; Reuter et al. 1993; Braine et al. 1995; Inoue et al. 1996; Bridges & Irwin 1998; Lim, Ao & Dinh-V-Trung 2008). Observations have now demonstrated that CO emission also extends to some tens of kpc from the central galaxy (Salomé et al. 2006, 2008a,b, 2011) and is strongly correlated with the filamentary struc-

ture observed in H α (Hu et al. 1983; Cowie et al. 1983; Conselice, Gallagher & Wyse 2001) within the hot gas detected in X-rays at 0.5 keV (Fabian et al. 2008). The H α structure is also correlated with warm H₂ emission (Edge et al. 2002; Wilman et al. 2002). Some of the molecular gas towards the cluster must be at high density ($\geq 10^4$ cm⁻³). Salomé et al. (2008a) have made the first detection of the high density tracer HCN(3-2) emission towards the centre of NGC 1275.

The nature of the filamentary structure is the subject of current discussion. Salomé et al. (2011) note two possibilities: either that the CO filaments form far from the galaxy's centre from uplifted warm gas, eventually falling back (Revaz, Combes & Salomé 2008), or that the molecular gas is entrained and dragged out of the galaxy by rising hot gas. Evidently, further observations of molecular gas may help to determine its origin. In this paper, we present observations of emission lines of CN(2-1), HCO⁺(3-2) and

* E-mail: eb@star.ucl.ac.uk;
twh@ast.leeds.ac.uk; sv@star.ucl.ac.uk

daw@star.ucl.ac.uk;

C₂H(3-2) towards the central galaxy and also towards a position 20'' to the east where there is strong CO emission in the associated filamentary structure.

These three species were identified in a theoretical study (Bayet et al. 2011) as tracers of regions influenced by the dissipation of turbulence and waves, heating the gas and accelerating cosmic rays (see also Crawford & Fabian 1992; Pope, Hartquist & Pittard 2008). Ferland et al. (2009) developed models of the optical and infrared emission filamentary regions in order to infer the rate at which mechanical energy is dissipated, and to determine the cosmic ray background produced by the interaction. Ferland et al. (2009) concluded that the heating rate per hydrogen nucleus due to dissipation or cosmic ray induced ionisation must be 300 times higher in the optical emission filaments than in the local interstellar medium.

In their work, (Bayet et al. 2011) identified the species CN, C₂H and HCO⁺ as sensitive to changes in cosmic ray ionisation rate or to an additional source of heating such as dissipation. Meijerink et al. (2011) came to a similar conclusion. Here, we present the observational follow-up to that theoretical study; we aim to determine whether dissipation or cosmic ray induced ionisation dominates the heating.

The paper is organised as follows: in Section 2 we present the first observations of CN(2-1), C₂H(3-2) and HCO⁺(3-2) emissions in both NGC 1275 and a position 20'' to the east where emission in the CO filamentary structure is known to be strong (see Figure 1). In Section 3 we analyse the data and provide rough estimates of column densities and fractional abundances of the three molecules in NGC 1275 and in the filamentary region. Section 4 compares the results of the observations with the models of Bayet et al. (2011) to try to identify whether cosmic ray heating or dissipation is the dominant heating mechanism, or whether a combination of both is required. Section 5 discusses the results and gives our conclusions.

2 OBSERVATIONS

The observations were performed using the James Clerk Maxwell Telescope (JCMT) for the detection of the CN(2-1) line ($\nu = 226.874$ GHz), C₂H(3-2) transition ($\nu = 262.004$ GHz) and HCO⁺(3-2) line ($\nu = 267.557$ GHz). In this first attempt of detection, we did not seek to resolve the fine structure line emission of the CN nor of the C₂H but rather observe the emission coming from the whole (2-1) and (3-2) group, respectively. Every two or three hours the pointing, focus and calibration were performed carefully on planets (Mars and Jupiter) and on evolved stars. The pointing error was estimated to be $\leq 3''$.

The JCMT observations were made between August and December 2010 under medium weather conditions ($\tau_{225} \approx 0.08-0.15$). We employed a beam switch mode with a throw of 95'' and used the RxA3 receiver on JCMT for detecting these three molecular emissions, coupled with the ACSIS digital autocorrelation spectrometer with a bandwidth of 1000MHz because the lines were expected to be broad (see Figures 1 and 3). The HPBW and the main beam

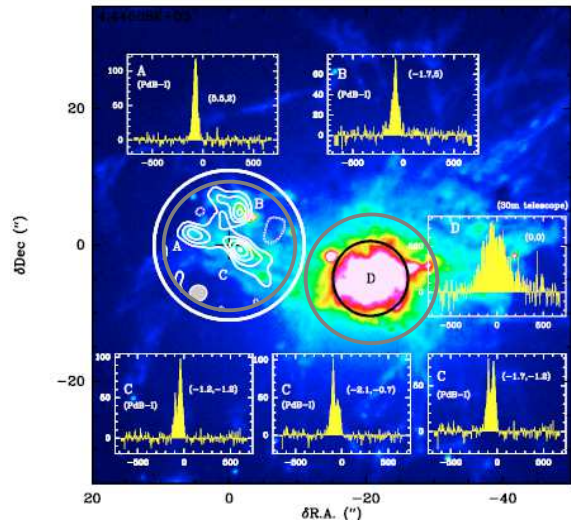


Figure 1. Extracted from Salomé et al. (2008b). This figure presents the positions and size of our JCMT beams (20'' grey circles) used for our observations relative to the integrated CO(2-1) intensity (white contours) seen on an H α image from Conselice, Gallagher & Wyse (2001) (colour scale) of NGC 1275. The white circle shows the Plateau de Bure Interferometer primary beam of the Salomé et al. (2008b) CO data. The black circle located on NGC 1275 (at (-20'', -5'') offsets from the centre on the map) corresponds to the 11.7'' beam of the IRAM-30m single-dish telescope CO data from Salomé et al. (2006).

efficiencies of the JCMT at $\nu \sim 250$ GHz are 20'' and 0.69¹, respectively (see the projected JCMT beam on Figure 1 as compared to the one corresponding to the published data from IRAM-30m and IRAM-Plateau de Bure Interferometer). The system temperatures ranged between 200 K and 450 K, depending on the source (either NGC 1275 or the filament) and on the wavelength. The data pre-reduction was done using Starlink software (KAPPA, SMURF and STLCONVERT packages) and subsequently translated to CLASS format for final reduction. The reduced spectra for NGC 1275 and the filamentary region are seen respectively in Figures 2 and 3 and their resulting Gaussian fitting parameters are displayed in Table 1.

The C₂H(3-2) line in NGC 1275 and the three lines observed in the filamentary region show a signal-to-noise ratio below the usual extragalactic cutoff of 3σ . For clear detections in the filamentary region, one would require more on-source integration time. These observations are thus to be considered all as upper limits, even though in the case of the C₂H(3-2) line in NGC 1275 and of the HCO⁺(3-2) and CN(2-1) transitions in the filament, Gaussian line profiles could be fitted to the observations (see Figures 2 and 3). Where fits could be obtained, the fitting parameters are shown in Table 1. However, note that for the lines of low signal-to-noise the values should be regarded, with caution, as indicative; these values are shown in *italic* in Table 1.

To correct the integrated line intensities for beam dilution effects, we have assumed optically thin emission (antennae temperature proportional to the column density in

¹ See JCMT website: <http://www.jach.hawaii.edu/JCMT/instruments/>

Table 1. Observational parameters and Gaussian fits parameters obtained for the data set. When the data are upper limits and we have not succeeded in fitting any Gaussian line profiles, we have used a symbol “–” in the table and given for the T_{peak} value a 3σ estimate based on the value of the observed rms. When fitting values are seen in a italic text font, it means that the observations are also to be considered as upper limits but it has been possible to fit a Gaussian line profile to the data (see text in Section 2).

	NGC 1275	Filament
RA(J2000) (h:m:s)	03:19:48.20	03:19:50.00
DEC(J2000) ($^{\circ}$: ' : ")	41:30:42.0	41:30:47.0
Position in Figure 1	D	A, B & C
HCO⁺(3-2), $\nu = 267.557$ GHz		
Tsys (K)	253	315
Integration time ^a (mins)	20	18
$\int(T_{mb} dv)$ (K km s ⁻¹)	18.3±0.4	<i>4.2±0.4</i>
V_{peak} (km s ⁻¹)	5178.7±5.0	<i>5185.7±11.1</i>
FWHM (km s ⁻¹)	437.5±10.0	<i>372.1±34.2</i>
T_{peak} (mK)	39.4	<i>10.5</i>
rms (mk)	7.9	8.6
CN(2-1), $\nu = 226.874$ GHz		
Tsys (K)	197	252
Integration time ^a (mins)	27	20
$\int(T_{mb} dv)$ (K km s ⁻¹)	5.9±0.2	<i>0.7±0.2</i>
V_{peak} (km s ⁻¹)	5197.3±4.3	<i>5248.9±33.5</i>
FWHM (km s ⁻¹)	275.9±9.5	<i>214.2±91.0</i>
T_{peak} (mK)	20.2	<i>3.0</i>
rms (mk)	4.8	2.8
C₂H(3-2), $\nu = 262.004$ GHz		
Tsys (K)	306	442
Integration time ^a (mins)	18	18
$\int(T_{mb} dv)$ (K km s ⁻¹)	<i>3.1±0.2</i>	-
V_{peak} (km s ⁻¹)	<i>5126.8±7.4</i>	-
FWHM (km s ⁻¹)	<i>180.8±17.3</i>	-
T_{peak} (mK)	<i>16.3</i>	<23.4
rms (mk)	8.3	7.8

^a The integration time listed here is the ON-SOURCE time only.

the upper level of the observed transition) and source sizes of 20'' and 11'' for NGC 1275 and the filament regions, respectively. These source sizes have been derived from the CO single-dish and interferometric maps from Salomé et al. (2006, 2008a,b) (see also Figure 1). We have applied this correction before estimating the column densities and fractional abundances (but note that the data in Table 1 do not include any correction for beam dilution).

We note that the HCO⁺(3-2) line in NGC 1275 is significantly broader than other lines presented here, and is broader than the CO(1-0) and CO(2-1) line widths (of about 380 km s⁻¹) reported in Bridges & Irwin (1998); Salomé et al. (2006, 2008a). The cause of this broadening is unclear. The range of frequencies covered by the spectrum seen in Figure 2 (i.e. 267.093-268.036 GHz), includes only one group of lines potentially strong enough to blend with the HCO⁺(3-2) emission and cause this broadening: this is the methanol emission located around 267.5 GHz. However, since methanol (in any frequency range) has not been detected in NGC 1275, nor has it been found in any central galaxy of a cluster, this possible explanation remains hypothetical.

Using previously published Perseus cluster molecular line data, we have listed in Table 2 some line ratios corrected for beam dilution effects. We have included additional molecular lines known to be reliable tracers of relatively high density gas from Bridges & Irwin (1998); Salomé et al. (2008a). For the filamentary region, we have used the CO(3-2) integrated line intensity from Bridges & Irwin (1998) at the position closest to ours ((+7'';+7'') as compared to (+20'';+5''), without finding a better match.

We briefly compare our results for the Perseus Cluster with the results of other molecular line studies of galaxies. Gao & Solomon (2004) give integrated line intensities (K km s⁻¹) for CO in nearby galaxies ranging from a few to a few hundred, while for HCN the values range from a few tenths to a few tens (see also Aalto et al. 2002). Our results (in the same units) for CN(2-1), C₂H(3-2) and HCO⁺(3-2) are 5.9, 3.1 and 18.3. So, in NGC 1275 these three molecular species are typically as bright as HCN in many other galaxies, though not as bright as CO.

Table 2. Line ratios using previously published data from Bridges & Irwin (1998); Salomé et al. (2006, 2008a) and the observations presented here. The line ratios have been calculated only after the integrated line intensities of all the observations used here were corrected for beam dilution effects using an assumed beam size of 20". When the symbol '-' is used, it means that the data are unknown. The CO(3-2) integrated line intensity used in the filamentary calculations from Bridges & Irwin (1998) does not correspond exactly to the position observed here and therefore has to be considered as a lower limit.

	NGC 1275	Filament
HCO ⁺ (3-2)/CO(3-2)	2.12	<0.53
HCO ⁺ (3-2)/HCN(3-2)	13.46	-
CN(2-1)/CO(3-2)	0.68	<0.09
CN(2-1)/HCN(3-2)	4.31	-
C ₂ H(3-2)/CO(3-2)	0.36	-
C ₂ H(3-2)/HCN(3-2)	2.28	-

3 COLUMN DENSITY AND FRACTIONAL ABUNDANCE ESTIMATES

To convert the integrated line intensities into column densities and fractional abundances, the hypothesis of a Local Thermodynamical Equilibrium (LTE) has been assumed such as, for a species X , we have:

$$N_{tot}(X) = \frac{N_u(X)}{g_u} \times Q(T_{rot}) \times \exp\left(\frac{E_u}{k \times T_{rot}}\right) \quad (1)$$

where $\frac{N_u}{g_u}(X)$ is defined by:

$$\frac{N_u}{g_u}(X) = 1.669 \times 10^{17} \times \frac{\int T_{mb} dv_{corr}}{\nu \times (S\mu^2)} \quad (2)$$

where $\int T_{mb} dv_{corr}$ corresponds to the integrated line intensities listed in Table 1, corrected from beam dilution effect, where $Q(T_{rot})$ is the partition function at the rotational temperature T_{rot} , where E_u is the energy of the upper level of the studied transition, where k is the Planck constant, and where $S\mu^2$ can be found, similarly to $Q(T_{rot})$ values, in the Cologne Database for Molecular Spectroscopy (CDMS²).

Any more sophisticated treatment at this stage of the observations has been considered as meaningless since only one transition per molecule has been obtained per source. Since the current dataset of observations does not allow us to estimate the rotational temperature T_{rot} i. e. rotational diagrams could not be constructed, we present in Table 3 values of the total column densities for CN, C₂H and HCO⁺ as functions of T_{rot} . The T_{rot} values listed have been chosen to be consistent with the range of kinetic temperatures computed self-consistently in the various models explored by Bayet et al. (2011).

To estimate the fractional abundance of a molecule from its estimated total column density, $N_{tot}(X)$ we have assumed the canonical gas:dust ratio for the Milky Way. This value may not be appropriate for the Perseus Cluster. We have selected A_v to be equal to either 3 mag or 8 mag. This allows the direct comparison with results presented in Bayet et al. (2011). Though we cannot be certain that the material is at either of these visual extinctions. However, we have selected

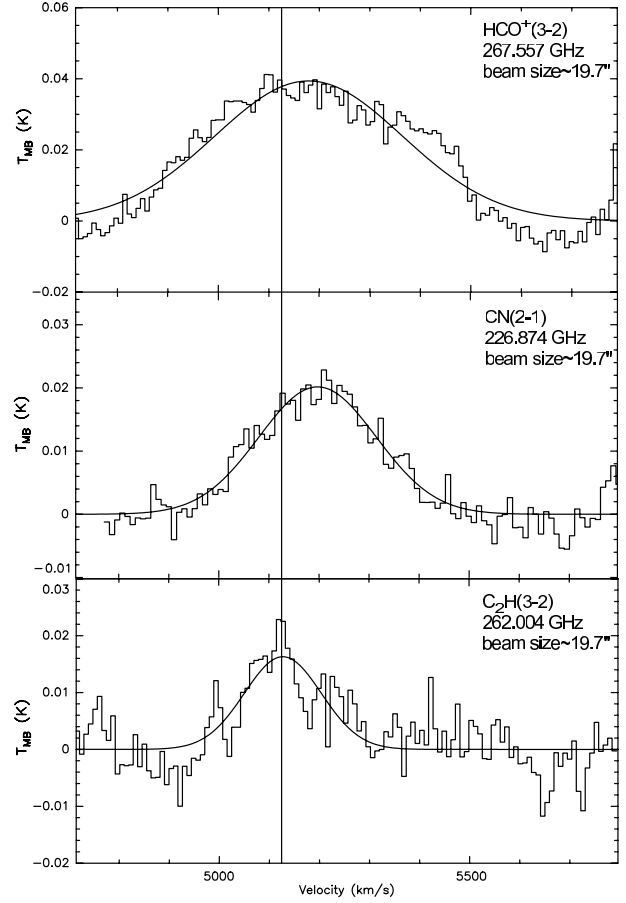


Figure 2. Molecular spectra obtained in NGC 1275, galaxy located at the centre of the Perseus cluster. *Top panel:* HCO⁺(3-2) line, *Middle panel:* CN(2-1) transition and *Bottom panel:* C₂H(3-2) line. The vertical black line represents the position of the $V_{lsr}=5125$ km s⁻¹ for the CO gas in NGC 1275 (see Bridges & Irwin 1998). In each panel, the back curve shows the result of the Gaussian fit profile applied whose output parameters are listed in Table 1 (see Section 2). Despite the fact that a Gaussian profile can be fitted to the C₂H(3-2) spectrum, this observation can not be considered as a detection since its corresponding signal-to-noise ratio is below the usual extragalactic cutoff of 3.

them as the lower value is representative of translucent regions and the higher corresponds to a dark region that does not have such a high column density that its lifetime would necessarily be significantly limited by gravitational collapse. We recognize that the whole procedure that we have used is necessarily very crude, but it does allow rough estimates of fractional abundances to be made, to compare with models (see Section 4). The derived column densities and fractional abundances, for both NGC 1275 and the filamentary region, are presented in Tables 3 and 4, respectively.

² See the website: <http://www.astro.uni-koeln.de/cgi-bin/cdmssearch>.

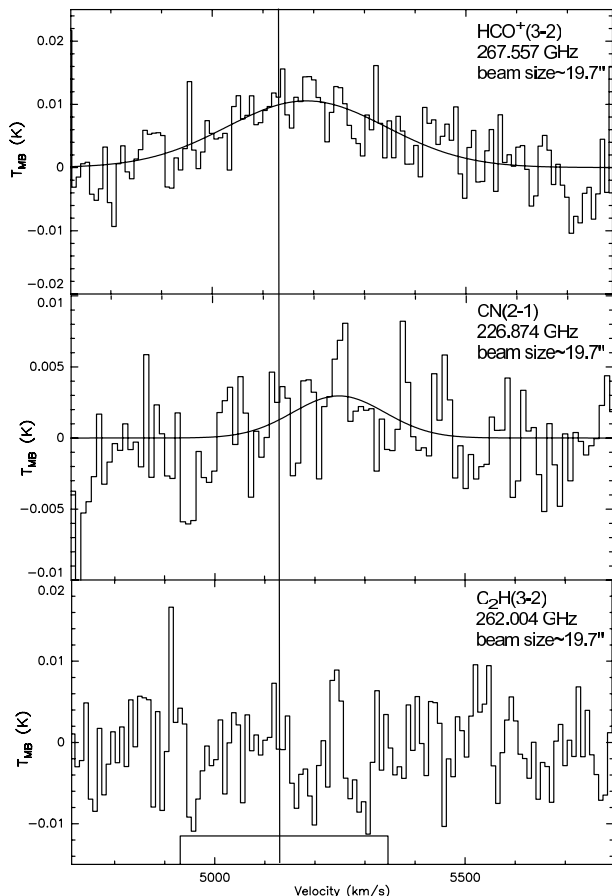


Figure 3. Molecular spectra obtained in a shifted position to the centre of the Perseus cluster corresponding to a filamentary structure. *Top panel:* $\text{HCO}^+(3-2)$ line, *Middle panel:* $\text{CN}(2-1)$ transition and *Bottom panel:* $\text{C}_2\text{H}(3-2)$ line. See caption of Figure 2. All the observations presented in this figures have to be considered as upper limits only, even if a Gaussian line profile can be seen for the $\text{HCO}^+(3-2)$ and the $\text{CN}(2-1)$ lines. Indeed, for these three observations, the signal-to-noise ratio obtained is actually below the usual extragalactic cutoff of 3. Any Gaussian fit seen has thus to be considered as only indicative of a *potential* detection. The velocity window seen on the spectrum of the $\text{C}_2\text{H}(3-2)$ line is indicative too, for marking the expected position of the line, if it were detected.

4 COMPARISON WITH MODEL PREDICTIONS: CONSTRAINTS ON THE ORIGIN OF THE HEATING MECHANISMS IN THE PERSEUS CLUSTER

We have extracted from Bayet et al. (2011), the values of the fractional abundances of CN, C_2H and HCO^+ from five models that may be appropriate for reproducing the observations presented here in both NGC 1275 and in the filament region. We present these values in Table 5. They offer five distinct combinations of cosmic ray ionisation rate (hereafter ζ in s^{-1}), of additional source of heating, H , (in $\text{erg cm}^{-3} \text{s}^{-1}$) accounting for the effect of dissipation, and of FUV radiation field, I , (expressed in units of Habing - see Habing 1968).

More precisely, Model A has high values of both H and ζ with a low value of I . Model B has low values of H , ζ and I . Model C has low values of H and ζ with a high value of

I . Model D has a high value of H and low values of ζ and I . Model E has a low value of H , a high value of ζ and a low value of I (See Table 5). Each model explored thermal and chemical properties at two values of A_v , i.e. $A_v = 3$ and 8 mag. These values are intended to represent conditions near the edge and in the dark interior of a molecular region.

By comparing directly the observed fractional abundances values presented in Table 4 with those modelled listed in Table 5, for the same temperature range (i.e. here, we compare only observed and modelled fractional abundances at $T_{\text{rot}} \sim T_K$), we may be able to identify which heating process may be present and consistent with the observed emissions of both NGC 1275 and the filamentary region. A summary of our conclusions is presented in Table 6. As one can see, there are actually a relatively limited number of models which can reproduce the observations well. Here we arbitrarily considered that a model reproduces well an observation when there is a factor of 5 or less between the modelled and observed fractional abundances. This factor has been selected such as taking into account possible uncertainties on the detections (e.g. pointing, calibration, etc) as well as uncertainties in the gas:dust ratio that affect the column densities and fractional abundances; also, the model results for abundances scale with the unknown metallicity.

Inspection of Table 6 suggests that the radiation field has little effect on the resulting chemistry, whatever values are attained by H and ζ . We shall ignore the FUV radiation field parameter in the following discussion, and focus on the effects of varying H and ζ . Note that where the observations supply only upper limits, we have assumed that the actual value is close to the upper limit. Further, we note that the success or failure of the models to match observations appears to be the same for both the centre, i.e. towards NGC 1275, and the eastern filamentary position.

Table 6 shows that individual species may have a match with observation for several models. For example, CN gives a match to observations for Models B, E (at $A_v = 3$ mag), Model D and Model C, while C_2H could match the observations for Models E and A. However, if all the molecules are assumed to share the same space and physical conditions, then we require a single model to account for all the species considered. Table 6 shows that there is such a model, Model E. It can account for CN and HCO^+ at $A_v = 3$ mag (though not at 8 mag), and for C_2H . The values of T_{rot} associated with all three molecules is 50 K. It is encouraging that the same value of T_{rot} applies to all three species. We discuss the implication of this finding in Section 5.

5 DISCUSSION AND CONCLUSIONS

The comparison in Section 4 between the molecular abundances obtained from the observations and from the models of Bayet et al. (2011) suggests that we can identify one model, Model E, that produces results consistent with the observations. This model has a low FUV radiation field, a low rate of heating by dissipation, but a high cosmic ray ionization rate. Unpublished data from the Bayet et al. (2011) calculations show that cosmic ray heating accounts for 85% of all heating at either $A_v = 3$ or 8 mag.

The enhanced cosmic ray flux may arise in a dynamical interaction, as suggested by Ferland et al. (2009). Those

authors also found that an enhanced cosmic ray ionization rate was required to account for the observations of the optical and infrared emitting components of the filaments. It is interesting, therefore, that the results from the present work also suggest that the regions of cluster gas probed by millimetre and sub-millimetre emissions also require a similarly enhanced cosmic ray ionization rate. A second inference is that a high heating rate from energy dissipation is not required; in fact, as Table 6 indicates, a high heating rate from sources other than cosmic rays appears to inhibit a match between models and observations.

In the observations, we have detected only one line in each of three molecular species, so a reliable analysis of the observational data cannot be made. It would be useful for the further study of galaxy cluster gas to make confirmed detections of several lines of each of the three molecular tracers used in this work. In the modelling of the chemistry of the gas in and around NGC 1275 (Bayet et al. 2011), some important physical parameters (e.g. gas:dust ratio and metallicity) are poorly known and undoubtedly have an impact on the model predictions. Nevertheless, the present work shows the value of molecular line observations of cluster gas, and it is interesting that the results reported here for the molecular gas are reasonably consistent with the results for regions probed by the optical and infrared. The main conclusions of this work are that a cosmic ray ionization rate enhanced by a factor of at least one hundred in the cluster gas is required to establish the observed molecular abundances, and that a high heating rate from other causes appears to mitigate against that chemistry. In these circumstances, the HCO^+ emission is strong.

ACKNOWLEDGMENTS

EB, TWH and SV acknowledges financial support from STFC. We thank Alastair Edge for his constructive referee's report, which helped us improve the paper.

REFERENCES

- Aalto S., Polatidis A. G., Hüttemeister S., Curran S. J., 2002, *A&A*, 381, 783
- Bayet E., Williams D. A., Hartquist T. W., Viti S., 2011, *MNRAS*, 639
- Braine J., Wyrowski F., Radford S. J. E., Henkel C., Lesch H., 1995, *A&A*, 293, 315
- Bridges T. J., Irwin J. A., 1998, *MNRAS*, 300, 967
- Conselice C. J., Gallagher, III J. S., Wyse R. F. G., 2001, *Aj*, 122, 2281
- Cowie L. L., Hu E. M., Jenkins E. B., York D. G., 1983, *ApJ*, 272, 29
- Crawford C. S., Fabian A. C., 1992, *MNRAS*, 259, 265
- Edge A. C., Wilman R. J., Johnstone R. M., Crawford C. S., Fabian A. C., Allen S. W., 2002, *MNRAS*, 337, 49
- Fabian A. C., Johnstone R. M., Sanders J. S., Conselice C. J., Crawford C. S., Gallagher, III J. S., Zweibel E., 2008, *Nature*, 454, 968
- Ferland G. J., Fabian A. C., Hatch N. A., Johnstone R. M., Porter R. L., van Hoof P. A. M., Williams R. J. R., 2009, *MNRAS*, 392, 1475
- Gao Y., Solomon P. M., 2004, *ApJ*, 606, 271
- Habing H. J., 1968, *Bul. of the Astron. Inst. of the Netherlands*, 19, 421
- Hu E. M., Cowie L. L., Kaaret P., Jenkins E. B., York D. G., Roesler F. L., 1983, *ApJ Letter*, 275, L27
- Inoue M. Y., Kameno S., Kawabe R., Inoue M., Hasegawa T., Tanaka M., 1996, *Aj*, 111, 1852
- Lazareff B., Castets A., Kim D.-W., Jura M., 1989, *ApJ Letter*, 336, L13
- Lim J., Ao Y., Dinh-V-Trung, 2008, *ApJ*, 672, 252
- Meijerink R., Spaans M., Loenen A. F., van der Werf P. P., 2011, *A&A*, 525, A119+
- Mirabel I. F., Sanders D. B., Kazes I., 1989, *ApJ Letter*, 340, L9
- Pope E. C. D., Hartquist T. W., Pittard J. M., 2008, *MNRAS*, 389, 1259
- Reuter H. P., Pohl M., Lesch H., Sievers A. W., 1993, *A&A*, 277, 21
- Revaz Y., Combes F., Salomé P., 2008, *A&A*, 477, L33
- Salomé P. et al., 2006, *A&A*, 454, 437
- Salomé P., Combes F., Revaz Y., Downes D., Edge A. C., Fabian A. C., 2011, *ArXiv e-prints*
- Salomé P., Combes F., Revaz Y., Edge A. C., Hatch N. A., Fabian A. C., Johnstone R. M., 2008a, *A&A*, 484, 317
- Salomé P., Revaz Y., Combes F., Pety J., Downes D., Edge A. C., Fabian A. C., 2008b, *A&A*, 483, 793
- Wilman R. J., Edge A. C., Johnstone R. M., Fabian A. C., Allen S. W., Crawford C. S., 2002, *MNRAS*, 337, 63

This paper has been typeset from a $\text{T}_{\text{E}}\text{X}/\text{L}^{\text{A}}\text{T}_{\text{E}}\text{X}$ file prepared by the author.

Table 3. Total column density estimates (in cm^{-2}) obtained using the formula described in Section 3, for various values of T_{rot} . Since there are observed upper limits for both NGC 1275 and the filamentary region, the corresponding derived total column densities presented here are thus also to be considered as upper limits (symbol $<$ used). The values of T_{rot} has been selected with respect to the available online values of the partition function $Q(T_{\text{rot}})$ and such as to be compatible with the range of kinetic temperature displayed by the models (see Table 5).

	$T_{\text{rot}} = 2.725 \text{ K}$	$T_{\text{rot}} = 5 \text{ K}$	$T_{\text{rot}} = 9.375 \text{ K}$	$T_{\text{rot}} = 18.75 \text{ K}$	$T_{\text{rot}} = 37.5 \text{ K}$	$T_{\text{rot}} = 50 \text{ K}$	$T_{\text{rot}} = 75 \text{ K}$
NGC 1275							
HCO ⁺	6.93×10^{14}	1.84×10^{13}	2.62×10^{12}	9.45×10^{11}	6.22×10^{11}	5.86×10^{11}	5.46×10^{11}
CN	2.42×10^{14}	1.91×10^{13}	5.02×10^{12}	2.53×10^{12}	1.93×10^{12}	1.86×10^{12}	1.79×10^{12}
C ₂ H	$< 9.03 \times 10^{15}$	$< 1.55 \times 10^{14}$	$< 1.74 \times 10^{13}$	$< 5.40 \times 10^{12}$	$< 3.23 \times 10^{12}$	$< 2.94 \times 10^{12}$	$< 2.66 \times 10^{12}$
Filament							
HCO ⁺	$< 2.10 \times 10^{14}$	$< 5.58 \times 10^{12}$	$< 7.94 \times 10^{11}$	$< 2.87 \times 10^{11}$	$< 1.88 \times 10^{11}$	$< 1.78 \times 10^{11}$	$< 1.66 \times 10^{11}$
CN	$< 4.68 \times 10^{14}$	$< 3.69 \times 10^{13}$	$< 9.70 \times 10^{12}$	$< 4.89 \times 10^{12}$	$< 3.73 \times 10^{12}$	$< 3.60 \times 10^{12}$	$< 3.36 \times 10^{12}$
C ₂ H	$< 1.34 \times 10^{16}$	$< 2.52 \times 10^{14}$	$< 2.97 \times 10^{13}$	$< 9.47 \times 10^{12}$	$< 5.74 \times 10^{12}$	$< 5.25 \times 10^{12}$	$< 4.77 \times 10^{12}$

Table 4. Fractional abundances (with respect to the total number of hydrogen nuclei) obtained using hypothesis described in Section 3, for various values of T_{rot} and for $A_v = 3 \text{ mag}$ and 8 mag (consistently with model predictions from Bayet et al. 2011. See text in Section 4). See caption of Table 3.

	$T_{\text{rot}} = 2.725 \text{ K}$	$T_{\text{rot}} = 5 \text{ K}$	$T_{\text{rot}} = 9.375 \text{ K}$	$T_{\text{rot}} = 18.75 \text{ K}$	$T_{\text{rot}} = 37.5 \text{ K}$	$T_{\text{rot}} = 50 \text{ K}$	$T_{\text{rot}} = 75 \text{ K}$
NGC 1275							
$A_v = 3 \text{ mag}$							
HCO ⁺	1.44×10^{-7}	3.84×10^{-9}	5.45×10^{-10}	1.97×10^{-10}	1.30×10^{-10}	1.22×10^{-10}	1.14×10^{-10}
CN	5.04×10^{-8}	3.97×10^{-9}	1.05×10^{-9}	5.27×10^{-10}	4.01×10^{-10}	3.87×10^{-10}	3.72×10^{-10}
C ₂ H	$< 1.88 \times 10^{-6}$	$< 3.23 \times 10^{-8}$	$< 3.62 \times 10^{-9}$	$< 1.12 \times 10^{-9}$	$< 6.72 \times 10^{-10}$	$< 6.12 \times 10^{-10}$	$< 5.54 \times 10^{-10}$
$A_v = 8 \text{ mag}$							
HCO ⁺	5.42×10^{-8}	1.44×10^{-9}	2.05×10^{-10}	7.39×10^{-11}	4.86×10^{-11}	4.58×10^{-11}	4.27×10^{-11}
CN	1.89×10^{-8}	1.49×10^{-9}	3.92×10^{-10}	1.98×10^{-10}	1.51×10^{-10}	1.45×10^{-10}	1.40×10^{-10}
C ₂ H	$< 7.06 \times 10^{-7}$	$< 1.21 \times 10^{-8}$	$< 1.36 \times 10^{-9}$	$< 4.22 \times 10^{-10}$	$< 2.52 \times 10^{-10}$	$< 2.29 \times 10^{-10}$	$< 2.08 \times 10^{-10}$
Filament							
$A_v = 3 \text{ mag}$							
HCO ⁺	$< 4.38 \times 10^{-8}$	$< 1.16 \times 10^{-9}$	$< 1.65 \times 10^{-10}$	$< 5.97 \times 10^{-11}$	$< 3.93 \times 10^{-11}$	$< 3.70 \times 10^{-11}$	$< 3.45 \times 10^{-11}$
CN	$< 9.74 \times 10^{-8}$	$< 7.68 \times 10^{-9}$	$< 2.02 \times 10^{-9}$	$< 1.02 \times 10^{-9}$	$< 7.76 \times 10^{-10}$	$< 7.50 \times 10^{-10}$	$< 7.00 \times 10^{-10}$
C ₂ H	$< 2.79 \times 10^{-6}$	$< 5.24 \times 10^{-8}$	$< 6.18 \times 10^{-9}$	$< 1.97 \times 10^{-9}$	$< 1.20 \times 10^{-9}$	$< 1.09 \times 10^{-9}$	$< 9.93 \times 10^{-10}$
$A_v = 8 \text{ mag}$							
HCO ⁺	$< 1.64 \times 10^{-8}$	$< 4.36 \times 10^{-10}$	$< 6.20 \times 10^{-11}$	$< 2.24 \times 10^{-11}$	$< 1.47 \times 10^{-11}$	$< 1.39 \times 10^{-11}$	$< 1.29 \times 10^{-11}$
CN	$< 3.65 \times 10^{-8}$	$< 2.88 \times 10^{-9}$	$< 7.58 \times 10^{-10}$	$< 3.82 \times 10^{-10}$	$< 2.91 \times 10^{-10}$	$< 2.81 \times 10^{-10}$	$< 2.62 \times 10^{-10}$
C ₂ H	$< 1.05 \times 10^{-6}$	$< 1.97 \times 10^{-8}$	$< 2.32 \times 10^{-9}$	$< 7.40 \times 10^{-10}$	$< 4.49 \times 10^{-10}$	$< 4.10 \times 10^{-10}$	$< 3.72 \times 10^{-10}$

Table 5. Predicted values of the fractional abundances (with respect to the total number of hydrogen nuclei) of CN, C₂H and HCO⁺ from models seen in Bayet et al. (2011). More precisely, Models A - E listed here correspond to Models 16, 14, 5, 18, and 12, respectively, in Bayet et al. (2011) hence to models having high values of both H and ζ with a low value of I ; low values of H , ζ and I ; low values of H and ζ with a high value of I ; high value of H and low values of ζ and I and low value of H , high value of ζ and low value of I , respectively. See the text in Section 4.

Model	A_v (mag)	T_K (K)	H (ergcm ⁻³ s ⁻¹)	ζ (s ⁻¹)	I (Habing)	Frac. abund. CN	Frac. abund. C ₂ H	Frac. abund. HCO ⁺
A	3	43.8	1.00×10^{-20}	5.00×10^{-15}	10	7.33×10^{-9}	3.32×10^{-10}	4.69×10^{-10}
A	8	47.5	1.00×10^{-20}	5.00×10^{-15}	10	7.24×10^{-9}	2.74×10^{-10}	5.94×10^{-10}
B	3	13.8	1.00×10^{-22}	5.00×10^{-17}	10	1.74×10^{-9}	9.01×10^{-12}	1.36×10^{-11}
B	8	14.9	1.00×10^{-22}	5.00×10^{-17}	10	1.81×10^{-10}	5.22×10^{-12}	5.32×10^{-11}
C	3	25.3	1.00×10^{-22}	5.00×10^{-17}	100	1.55×10^{-9}	5.50×10^{-11}	1.31×10^{-11}
C	8	14.5	1.00×10^{-22}	5.00×10^{-17}	100	1.82×10^{-10}	5.28×10^{-12}	5.16×10^{-11}
D	3	74.8	1.00×10^{-20}	5.00×10^{-17}	10	2.51×10^{-9}	8.82×10^{-11}	1.65×10^{-10}
D	8	63.3	1.00×10^{-20}	5.00×10^{-17}	10	8.61×10^{-10}	5.43×10^{-12}	2.62×10^{-10}
E	3	51.0	1.00×10^{-22}	5.00×10^{-15}	10	1.82×10^{-9}	2.68×10^{-10}	1.37×10^{-10}
E	8	60.2	1.00×10^{-22}	5.00×10^{-15}	10	1.99×10^{-9}	2.95×10^{-10}	2.94×10^{-10}

Table 6. Summary of the conclusions obtained when comparing the estimates of the fractional abundances derived from the observations to the model predictions (see Section 4). We have assumed that models and observations are in agreement (symbol ‘+’ used) when their values differ from less than or equal to a factor of 5 difference. Otherwise, the symbol ‘-’ is used. ‘(3)’ or ‘(8)’ means that the fractional abundances at $A_v = 3$ mag or at $A_v = 8$ mag are well reproduced by the models (but not at both A_v s), respectively.

Model Parameters	C ₂ H centre	C ₂ H filament	CN centre	CN filament	HCO ⁺ centre	HCO ⁺ filament
Model A: I low, H high, ζ high	+	+	-	-	(3)	-
Model B: I low, H low, ζ low	-	-	+	+	(8)	(8)
Model C: I high, H low, ζ low	-	-	+	+	(8)	(8)
Model D: I low, H high, ζ low	-	-	+	+	(3)	(3)
Model E: I low, H low, ζ high	+	+	(3)	(3)	(3)	(3)